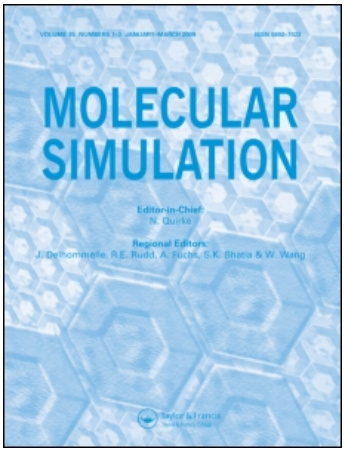

Molecular Simulation
Publication details, including instructions for authors and subscription information:
http://www.informaworld.com/smpp/title~content=t713644482

Examination of nanoflow in rectangular slits

W. Zhang[a]; D. Xia[a]
[a] School of Civil Engineering and Mechanics, Yanshan University, Qinhuangdao, Hebei Province, P. R. China

Online publication date: 27 July 2010

To cite this Article Zhang, W. and Xia, D.(2007) 'Examination of nanoflow in rectangular slits', Molecular Simulation, 33: 15, 1223 — 1228
To link to this Article: DOI: 10.1080/08927020701713886
URL: http://dx.doi.org/10.1080/08927020701713886

Molecular Simulation, Vol. 33, No. 15, December 2007, 1223–1228

Taylor & Francis
Taylor & Francis Group

Examination of nanoflow in rectangular slits

W. ZHANG* and D. XIA

School of Civil Engineering and Mechanics, Yanshan University, Qinhuangdao, Hebei Province 066004, P. R. China

(Received July 2007; in final form September 2007)

This paper presents simulations of 3D nanoscale flow in rectangular channel with molecular dynamics simulation method. Rectangular cross section is a frequently encountered geometric shape for nanoscale flow problems. For a given cross sectional height h, we change the width w of the rectangular cross section and analyze the influence of w/h on the flow characteristics. The distributions of density, temperature, boundary slip and flow velocity inside the rectangular cross section are investigated in detail. Liquid argon material and Lennard-Jones potential are used in the simulations. The simulation results are also compared with Navier–Stokes solutions for rectangular channel flows.

Keywords: Molecular dynamics simulation; Nanoscale flow; Rectangular channel; Multi-constraints

PACS: 47.45.Dt; 47.11. + j; 83.10.Rp

1. Introduction

Geometric shape of cross section of a pipe will affect the dynamic flow characteristics inside the pipe. In this aspect, for macro flows, exhausted studies have been exerted on both theoretical and numerical solution methods. Mortensen [1] derived the analytical relation between pressure drop and volume flow rate for channels with various different cross sectional shapes. In recent years, microfluidics and nanofluidics have been paid much attention. Usually, the continuum model is still used in micro flow problems but the flow characteristics are more sensitive to the cross sectional shape of the micro channel than that of the macro flows. When the dimension of the computational domain is several nanometers the continuum description of the medium is not available. The traditional solution methods for macroscale problems, based on differential equations, such as finite element method, finite difference method and finite volume method, etc. cannot be used. So, for nanoscale flows, particle methods are implemented, such as molecular dynamics simulation (MDS) or Monte Carlo simulation methods.

Since the theory of non-equilibrium molecular dynamics (NEMD) [2,3] is adopted various nanoscale flow problems are simulated and useful conclusions are reached. Velocity profile in nanoscale channels is an important part of nanoflow problems. Koplik *et al.* [4] studied Poiseuile flow; Travis *et al.* [5,6] compared the results of NEMD with the solutions of the Navier–Stokes (NS) equations. Nonlinear distributions of mass and viscosity are special features for nanoscale flows. Todd *et al.* presented their MDSs in Ref. [7]. Boundary slip is another important phenomenon in fluid mechanics. Quantitative analysis of boundary slip is useful for both macroscale and nanoscale flows. Heinbuch and Fischer [8] discussed slip boundary conditions of nanoscale liquid flow; Thompson and Robbins [9] presented detail analysis about the boundary conditions with different solid wall materials and interaction strength parameters. Hendy *et al.* [10] derived analytic boundary slip expressions suitable for different dimensions. Qian *et al.* [11] investigated the influence of Navier boundary slip conditions on Newtonian stress. With the increase of computer speed, more and more complicated and practical nanoscale flows can be resolved. References [12,13] are good reviews regarding the models, solution methods and applications of nanoscale flows.

Up to now, most MDS papers regarding nanoscale pipe flows consider pipes with circular cross sections. Flow between two infinite plates is also studied but it is usually replaced by a simplified two-dimensional model. Flows in a rectangular channels are frequently encountered in engineering equipments. For nanoscale flow the boundary influence of geometric shape is significant and there must

*Corresponding author. Tel.: + 86-335-8388506. Fax: + 86-335-8057101. Email: zwenfei@gmail.com

Molecular Simulation
ISSN 0892-7022 print/ISSN 1029-0435 online © 2007 Taylor & Francis
http://www.tandf.co.uk/journals
DOI: 10.1080/08927020701713886

be some new features worth to be explored. To reveal the intrinsic features of rectangular channel flows is the purpose of this work.

This paper simulates an equivalent gravity-driven 3D flow in pipes with rectangular cross sections. We fix the height and change the width of the rectangular cross sections. The flow velocity, temperature, boundary slip and mass distributions inside the rectangular cross sections are investigated. In these simulations, the material is liquid argon and Lennard-Jones potential is used. We also compared the MDS results and the no-slip NS solutions for rectangular channel flows.

2. Model of simulations

We consider a straight channel with constant rectangular cross section. Figure 1 shows the rectangular cross section of the channel, where h and w are the height and the width of the rectangular cross section, respectively. Let z represents the direction of flow. L is the length of the computational domain. In this figure, the solid circle ● represents the wall particles and the hollow circle ○ represents the fluid particles.

We fix the height h and change the width w to get different cases. Four cases are considered. Figure 2 shows the relation between w and h of each case.

Three layers of solid particles are placed to represent the solid wall. Initially, both the fluid particles and the particles of the solid wall are positioned in fcc lattices [14]. In the z direction, outside of the computational domain, we use periodic boundary conditions [14]. The physical problem is an isothermal gravity-driven steady 3D flow in the straight channel. The material is liquid argon and Lennard-Jones potential function (1) is used.

$$\phi(r_{ij}) = 4\varepsilon\left[\left(\frac{\sigma}{r_{ij}}\right)^{12} - \left(\frac{\sigma}{r_{ij}}\right)^{6}\right] \tag{1}$$

where $\phi(r_{ij})$ is the potential energy between the ith particle and the jth particle; $r_{ij} = |\mathbf{r}_i - \mathbf{r}_j|$ is the scalar distance between two molecules; $\mathbf{r}_i$ and $\mathbf{r}_j$ are the position vectors of the ith particle and the jth particle, respectively; σ is the length scale of a particle; ε is the strength parameter of the interaction. The interaction force between the ith particle and the jth particle is $\mathbf{F}_{ij} = -\nabla\phi(r_{ij})$. The movement

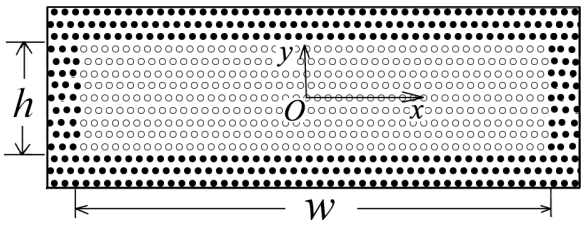

Figure 1. The rectangular cross section of the channel flow model. w and h are width and height of the cross section, respectively. ● represents the wall particles. ○ represents the fluid particles.

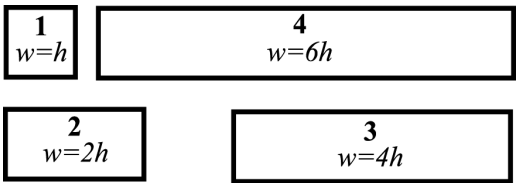

Figure 2. The relation of w and h of our four cases: case 1, $w = h$; case 2, $w = 2h$; case 3, $w = 4h$; case 4, $w = 6h$.

equations for the ith fluid particle are

$$\dot{\mathbf{r}}_i = \frac{\mathbf{p}_i}{\mathrm{m}_i} \tag{2}$$

and

$$\dot{\mathbf{p}}_i = \mathbf{F}_i + \mathbf{F}_i^{\mathrm{e}} - \alpha\left[\frac{\mathbf{p}_i}{\mathrm{m}_i} - \mathbf{u}(\mathbf{r}_i, t)\right], \tag{3}$$

where $\mathbf{p}_i$ is the peculiar momentum of the ith particle, $\mathbf{F}_i$ is total interaction force exerted on the ith particle by all the other particles, $\mathbf{F}_i^{\mathrm{e}}$ is the external force exerted on the ith particle, $\mathbf{u}(\mathbf{r}_i, t)$ is the flow velocity of the fluid at point $\mathbf{r}_i$, α is a thermostat multiplier that will keep the system temperature constant. In equation (3), $\mathbf{u}(\mathbf{r}_i, t)$ is not the solution of the Stokes equations. It is the flow velocity statistically calculated based on the time average conception of particle velocity $\mathbf{v}_i$. $\mathbf{u}(\mathbf{r}_i, t)$ is a macro quantity of the fluid. It is calculated at each time step. When calculate the system temperature, for each particle, the flow velocity should be subtracted from the total velocity. When we simulate a steady flow, the flow velocity should not be a function of time variable t. From the point of view of molecular dynamics, at each time step, the particle velocity is different and the calculated flow velocity will have some changes. Certainly, statistically the flow velocity will reach a steady value. But it needs a period of time or many time steps to reach the steady state. During the process, the flow velocity is still a function of time variable t. Equations (2) and (3) are typical equations in NEMD for flow problems [12,15].

Equation (3) is the usual way to control the average temperature of the system. Because in this method the system temperature is controlled by only one parameter α, we call it single-constrained method. If the dimension of the simulated system is very small the single-constrained method can be adopted. However, if the dimension of the considered system is not small and the temperature distribution of the system is complicated, only one parameter is not enough to satisfy specific conditions.

To improve the ability to regulate the temperature distribution in the conventional constant temperature method Zhang [16] extended equation (3) to a more generalized form. In Ref. [16] the computational domain Ω is divided into M sub-domains. There are N_j particles in each sub-domain Ω_j,

$$\Omega = \sum_{j=1}^{M} \Omega_j, \quad N = \sum_{j=1}^{M} N_j$$

For each sub-domain an independent constant temperature constraint is imposed. Therefore, in sub-domain Ω_j, equation (3) is changed to

$$\dot{\mathbf{p}}_i = \mathbf{F}_i + \mathbf{F}_i^{\mathrm{e}} - \alpha_j \left[\frac{\mathbf{p}_i}{\mathrm{m}_i} - \mathbf{u}(\mathbf{r}_i, t) \right]. \tag{4}$$

The constant temperature condition in sub-domain Ω_j is

$$\sum_{i=1}^{N_j} \frac{\mathrm{m}_i}{2} \left[\frac{\mathbf{p}_i}{\mathrm{m}_i} - \mathbf{u}(\mathbf{r}_i, t) \right] \cdot \left[\frac{\mathbf{p}_i}{\mathrm{m}_i} - \mathbf{u}(\mathbf{r}_i, t) \right] = \frac{3}{2} N_j k T_j = \text{constant}, \tag{5}$$

where T_i is the average temperature in sub-domain Ω_j, α_j is a thermostat multiplier that will maintain the sub-domain Ω_j in constant temperature, k is Boltzmann's constant. The total kinetic energy of the system is the sum of the kinetic energy in all sub-domains

$$E = \sum_{j=1}^{M} \frac{3}{2} N_j k T_j. \tag{6}$$

The expression of α_j is

$$\alpha_j = -\sum_{i=1}^{N_j} \left[\frac{\mathbf{p}_i}{\mathrm{m}_i} - \mathbf{u}(\mathbf{r}_i, t) \right] \cdot \left(\frac{\partial \phi}{\partial \mathbf{r}_i} - \mathbf{F}_i^{\mathrm{e}} \right) \Big/ \sum \left[\frac{\mathbf{p}_i}{\mathrm{m}_i} - \mathbf{u}(\mathbf{r}_i, t) \right] \cdot \left[\frac{\mathbf{p}_i}{\mathrm{m}_i} - \mathbf{u}(\mathbf{r}_i, t) \right]. \tag{7}$$

Because the system temperature is controlled by several parameters α_j this algorithm is called multi-constrained method. In our simulations, the multi-constrained method can make the temperature distribution more reasonable. The details of the multi-constrained method are given in Ref. [16].

For the ith wall particle the movement equation (3) becomes

$$\dot{\mathbf{p}}_i = \mathbf{F}_i - \kappa(\mathbf{r}_i - \mathbf{r}_{0i}) - \alpha_j \frac{\mathbf{p}_i}{\mathrm{m}_i}. \tag{8}$$

Here, we assume that each wall particle is connected to its original position with springs in different directions and each wall particle vibrates about its original lattice site. The second term at the right hand side of (8) defines the spring force and κ is a stiffness coefficient of the springs, $\mathbf{r}_{0i}$ is the original position of the ith particle. We can adjust the value of κ to keep the amplitude of the vibration small. This method is suggested by Heinbuch *et al.* [8]. The last term at the right hand side of (8) is also a temperature constraint. In equations (4) and (8), α_j is a constant parameter at each time step. It is not a function of coordinates. But in different time steps α_j is different. That means α_j is a function of time variable t. We can get the explicit expression of α_j according to constant temperature condition. Details are given in Refs. [17,18]. Using leap-frog [14] numerical integration method, we calculate the peculiar velocity of each particle. Then, based on the time average conception, we can get the flow velocity, density and temperature distributions [14].

3. Navier–Stokes solution in a rectangular channel

Some times to analyze the difference between macro solution and the MDS solution is necessary. For the convenience of comparison, we derive the analytical solution of the Poisseuille flow as follows.

For steady flows of an incompressible Newtonian fluid in a straight rectangular channel with constant cross section, the NS equations are simplified to Stokes equation. That is, in this case, both the NS equations and the Stokes equation have the same form. The NS equations are simplified to

$$\frac{1}{\eta} \frac{\partial p}{\partial z} = \frac{\partial^2 u}{\partial x^2} + \frac{\partial^2 u}{\partial y^2}. \tag{9}$$

The no-slip boundary conditions are

$$u|_{x=-w/2} = 0, u|_{x=w/2} = 0$$
$$u|_{y=-h/2} = 0, u|_{y=h/2} = 0, \tag{10}$$

where u is the flow velocity in the z direction, p is the fluid pressure, η is the viscosity of the fluid. For a specific z, the pressure gradient $(1/\eta)(\partial p/\partial z)$ is a constant. In Poisson's equation (9), assume that the solution has the following form

$$u(x, y) = \sum_{i=1}^{\infty} \sum_{j=1}^{\infty} A_{ij} \cos \frac{(2i-1)\pi}{w} x \cos \frac{(2j-1)\pi}{h} y. \tag{11}$$

This solution satisfies the given boundary conditions (10). Substitute (11) into equation (9) we have

$$-\sum_{i=1}^{\infty} \sum_{j=1}^{\infty} A_{ij} \left[\left(\frac{(2i-1)\pi}{w} \right)^2 + \left(\frac{(2j-1)\pi}{h} \right)^2 \right] \cos \frac{(2i-1)\pi}{w} x \cos \frac{(2j-1)\pi}{h} y = \frac{1}{\eta} \frac{\partial p}{\partial z}. \tag{12}$$

After some manipulations, we get

$$A_{ij} = \frac{-1}{\left(\left(\frac{(2i-1)\pi}{w} \right)^2 + \left(\frac{(2j-1)\pi}{h} \right)^2 \right)} \frac{4}{wh} \times \int_{-w/2}^{w/2} \left[\int_{-h/2}^{h/2} \frac{1}{\eta} \frac{\partial p}{\partial z} \cos \frac{(2j-1)\pi}{h} y \, \mathrm{d}y \right] \times \cos \frac{(2i-1)\pi}{w} x \, \mathrm{d}x = \frac{-16 \times (-1)^{(i+j)}}{\left(\left(\frac{2i-1}{w} \right)^2 + \left(\frac{2j-1}{h} \right)^2 \right) (2i-1)(2j-1)\pi^4} \frac{1}{\eta} \frac{\partial p}{\partial z}, \tag{13}$$

The eventual form of velocity distribution function of a steady flow in a straight rectangular channel is

$$u(x,y) = \frac{1}{\eta}\frac{\partial p}{\partial z}\sum_{i=1}^{\infty}\sum_{j=1}^{\infty} \times \frac{-16\times(-1)^{(i+j)}}{\left(\left(\frac{2i-1}{w}\right)^2+\left(\frac{2j-1}{h}\right)^2\right)(2i-1)(2j-1)\pi^4} \times \cos\frac{(2i-1)\pi}{w}x\cos\frac{(2j-1)\pi}{h}y. \quad (14)$$

In the above velocity function, if we let $w \to \infty$ and $x = 0$ then function (14) is equivalent to the two-dimensional Poisseuille flow solution (15).

$$u(y) = -\frac{1}{2\eta}\frac{\partial p}{\partial z}\left(\left(\frac{h}{2}\right)^2 - y^2\right) \quad (15)$$

4. Simulations of channel flows

In our simulations, $h = 2.59 \times 10^{-9}$ m and $L = 26.52 \times 10^{-9}$ m. There are N_f fluid particles and N_w wall particles inside the computational domain, respectively. For the first case, we call it case 1, $w = h$, $N_f = 3726$, $N_w = 6624$; for case 2, $w = 2h$, $N_f = 7038$ and $N_w = 8832$; for case 3, $w = 4h$, $N_f = 13{,}662$ $N_w = 13{,}248$; and for case 4, $w = 6h$, $N_f = 20{,}286$, $N_w = 17{,}664$. We assume that the external force exerted on fluid particle i is $m_i\mathbf{g}_i$. Here, $\mathbf{g}_i$ is the given equivalent gravity acceleration vector. In our channel flow problem, $\mathbf{g}_i = \{0, 0, g_z\}$, where g_z is the equivalent gravity acceleration in the z direction. The initial velocity is given by the original temperature. The cut off radius is taken as $r_c = 2.5\sigma$. The interaction between the liquid and the solid wall is considered by the interaction strength parameter of the wall particles and the liquid particles. The values of the parameters used in the simulations are: the size of the particles $\sigma_f = \sigma_w = 3.4 \times 10^{-10}$ m; the mass of the particles $m_f = m_w = 6.69 \times 10^{-23}$ g; the temperature $T = 84$ K, corresponding to the liquid state of argon; the interaction strength parameter between argon molecules is $\varepsilon_f = 1.656 \times 10^{-21}$ kg m^2 s^{-2}; $g_z = (0.685\varepsilon_f)/(\sigma_f m_f)$; the stiffness coefficient of the springs is $\kappa = \varepsilon_f \times 10^3$. Here, the subscript f represents fluid and the subscript w represents solid wall. In our simulations, the size of each time step is chosen as $\Delta t = 10^{-14}$ s and leap-frog numerical integration algorithm is adopted. In principle, we can use different interaction strength parameter ε_w to represent different solid wall materials [19]. We used $\varepsilon_w = \varepsilon_f$ in our simulations. The interaction strength parameter for the interaction between a wall particle and a fluid particle ε_{wf} can be evaluated [19] by $\varepsilon_{wf} = (\varepsilon_f\varepsilon_w)^{1/2}$. For the multi-constrained algorithm, we averagely divide the width w into ten parts and then obtain ten sub-domains.

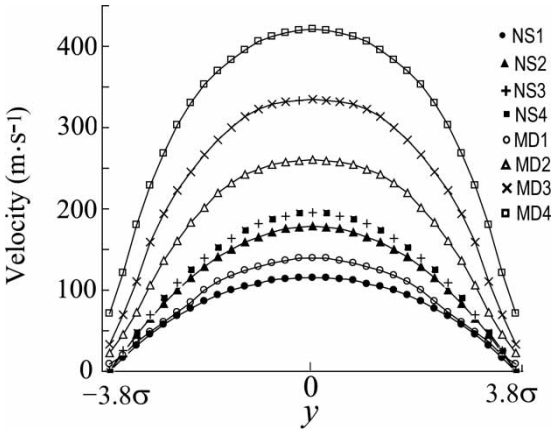

Figure 3. Velocity profile along the line $x = 0$. The vertical coordinate is the flow velocity (m s^{-1}) and the horizontal coordinate is y. NS1 represents the NS solution of case 1, MD1 represents the MD result of case 1, etc.

The velocity profiles calculated in our simulations are plotted in figures 3 and 4. In these figures, the NS solutions for the four cases are calculated from (10). Figure 3 is the velocity profile along the line $x = 0$. With the increase of width w the difference between the NS solution and the corresponding MD solution is also increased. Certainly this velocity difference is not only because the boundary slip. It is seen that, for each case, the difference between the maximum velocity of NS solution and the maximum velocity of MD simulation is bigger than the corresponding difference of boundary slips. In this figure, the NS solutions of case 3 and case 4 are overlapped and they are equal to the two-dimensional NS solution (11). This means when $w \geq 4h$, for the NS equations, we can use two-dimensional solution (11) to replace three dimensional solution (10). This conclusion is not true for nanoscale flow. From figure 3 we see that the simulation results of case 3 and case 4 are different. Figure 4 is the velocity profile along the line $y = 0$. When $-h < x < h$, lines of the NS and the MD solutions of case 4 are almost horizontal. It means that, on the line $y = 0$, at the point $2h$ from the boundary, the velocity will reach its maximum. This conclusion is hold for both the NS and the MD

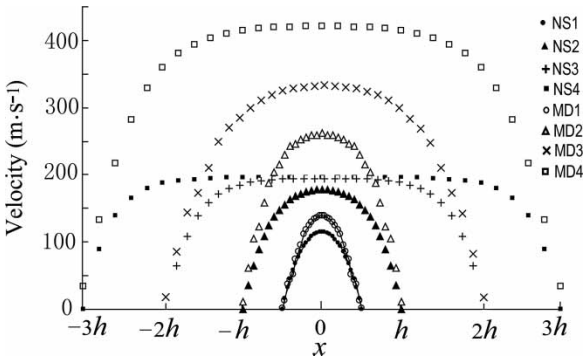

Figure 4. Velocity profile along the line $y = 0$. The vertical coordinate is the flow velocity (m s^{-1}) and the horizontal coordinate is x. NS1 represents the NS solution of case 1, MD1 represents the MD result of case 1, etc.

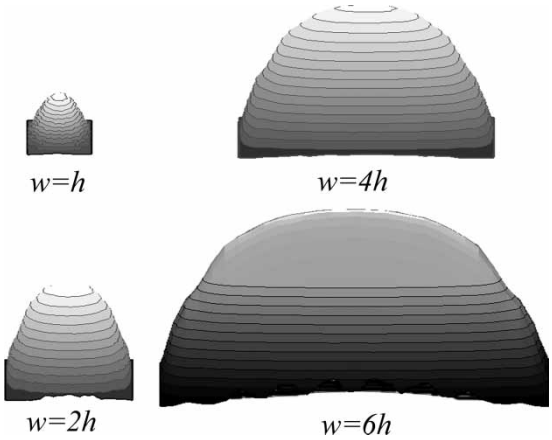

Figure 5. Contours of velocity distribution in the cross section of the four cases.

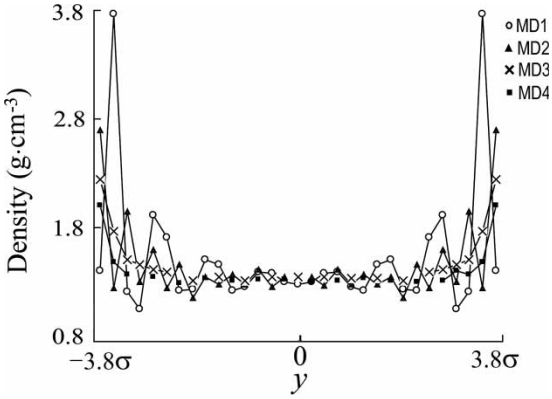

Figure 6. Density distribution along the line $x = 0$. The vertical coordinate is the density ($g\,cm^{-3}$) of the fluid and the horizontal coordinate is y. MD1 represents the MD result of case 1, MD2 represents the MD result of case 2, etc.

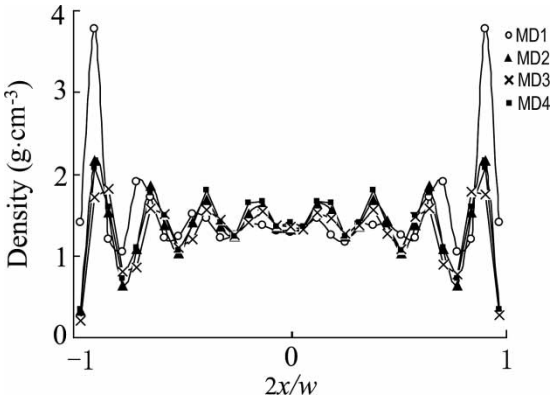

Figure 7. Density distribution along the line $y = 0$. The vertical coordinate is the density ($g\,cm^{-3}$) of the fluid and the horizontal coordinate is $2x/w$. MD1 represents the MD result of case 1, MD2 represents the MD result of case 2, etc.

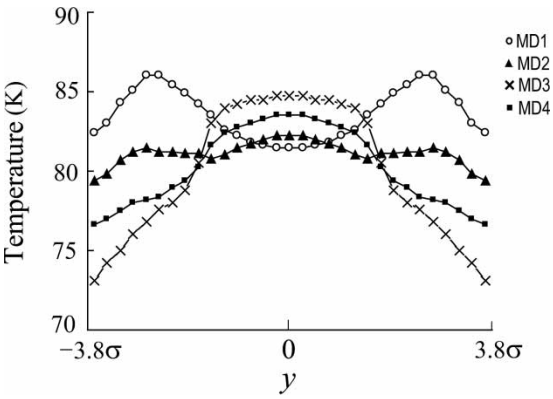

Figure 8. Temperature distribution along the line $x = 0$. The vertical coordinate is the temperature (K) of the fluid and the horizontal coordinate is y. MD1 represents the MD result of case 1, MD2 represents the MD result of case 2, etc.

solutions. The maximum velocity of MD simulation should also converge to a limit, but in our simulated models, the width, even for the $w = 6h$ case, is not big enough to reach the limit. This result also shows that the convergent speed is different between the MD and the analytical solutions. Figure 5 is the contours of velocity distribution in the cross sections of the four cases.

Figures 6 and 7 are density distributions along the lines $x = 0$ and $y = 0$, respectively. It is known that the density value will have drastic change near the wall boundary just as shown in figures 6 and 7. But, with the increase of w, the amplitudes of vibration of density function will decrease.

The temperature profile along the lines $x = 0$ is plotted in figure 8. We see that, in this figure, the temperature discrepancies between boundary point and the center point are obvoious for case 3 and case 4. It is because the flow velocities of case 3 and case 4 are large. The boundary temperature is smaller than the corresponding center temperature for case 3 and case 4. The similar phenomenon can also be seen from figure 9, the temperature profile along the lines $y = 0$. But, in figure 9, the boundary temperature is bigger than the corresponding center temperature for each case. It means, for nanoflows, the temperature distribution will be influenced by flow velocity and geometric shape of cross section.

5. Conclusions

This work simulates 3D steady flows in nanochannels with rectangular cross section. The boundary slip, velocity,

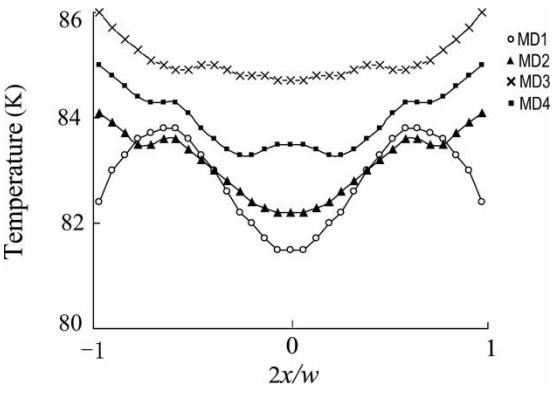

Figure 9. Temperature distribution along the line $y = 0$. The vertical coordinate is the temperature (K) of the fluid and the horizontal coordinate is $2x/w$. MD1 represents the MD result of case 1, MD2 represents the MD result of case 2, etc.

density and temperature distributions are analyzed. The velocity profiles are also compared with the NS solutions. The width w of the rectangular cross section has important influence on the flow characteristics. For the NS equations if w is great than $4h$ we can use 2D model to replace 3D model and get the same velocity distribution on the line $x = 0$. If the width w is big, on the line $y = 0$, at the point $2h$ from the boundary, the velocities will reach the maximum for both the NS and the MD solutions. The increase of w will make the amplitudes of vibration of density function smaller. The temperature distribution is totally different in the x and y directions if $w > h$. The shape of the temperature curves are affected by the value of the flow velocity.

Acknowledgements

This work was supported by grants from the Yanshan University, China.

References

[1] N.A. Mortensen, F. Okkels, H. Bruus. Reexamination of Hagen–Poiseuille flow: shape-dependence of the hydraulic resistance in microchannels. *Phys. Rev. E.*, **71**, 057301 (2005).
[2] S. Nose. A unified formulation of the constant temperature molecular dynamics methods. *J. Chem. Phys.*, **81**, 511 (1984).
[3] W.G. Hooer. Canonical dynamics: Equilibrium phase–space distributions. *Phys. Rev.*, **31**, 1695 (1985).
[4] J. Koplik, J.R. Banavar, J.F. Willemsen. Molecular dynamics of Poiseuile flow and moving contact line. *Phys. Rev. Lett.*, **60**, 1282 (1988).
[5] K.R. Travis, B.D. Todd, J.E. Denis. Departure from Navier–Stokes hydrodynamics in confined liquids. *Phys. Rev.*, **55**, 4288 (1997).
[6] K.P. Travis, K.E. Gubbins. Poiseuille flow of Lennard-Jones fluids in narrow slit. *J. Chem. Phys.*, **112**, 1984 (2000).
[7] B.D. Todd, D.J. Evans, P.J. Daivis. Pressure tensor for inhomogeneous fluids. *Phys. Rev. E*, **52**, 1627 (1995).
[8] U. Heinbuch, J. Fischer. Liquid flow in pores: slip, no-slip or multiplayer sticking. *Phys. Rev. A*, **40**, 1144 (1989).
[9] P.A. Thompson, M.O. Robbins. Shear flow near solids: epitaxial order and flow boundary conditions. *Phys. Rev. A*, **41**, 6830 (1990).
[10] S.C. Hendy, M. Jasperse, J. Burnell. The effect of patterned slip on micro and nanofluidc flows. *Phys. Rev. E.*, **72**, 016303 (2005).
[11] T. Qia, X. Wang. Driven cavity flow: from molecular dynamics to continuum hydrodynamics. *Multiscale Modeling Simul.*, **3**(4), 749 (2005).
[12] B.D. Todd. Computer simulation of simple and complex atomistic fluids by nonequilibrium molecular dynamics techniques. *Comput. Phys. Commun.*, **142**, 14 (2001).
[13] N. Giordano, J.T. Cheng. Microfluid mechanics: progress and opportunities. *J. Phys.: Condensed Matter*, **13**(15), 271 (2001).
[14] D.C. Rapaport. *The Art of Molecular Dynamics Simulation*, p. 16, Cambridge University press, Cambridge (1995).
[15] X. Mi, A.T. Chwang. Molecular dyanamics simulations of nanochannel flow at low reynolds numbers. *Molecules*, **8**, 193 (2003).
[16] W. Zhang. Multi-constraints in constant temperature molecular dynamics simulations. *Chem. Phys. Lett.*, **439**, 219 (2007).
[17] L. Zhang, R. Balasundaram, S.H. Gehrke, S. Jiang. Nonequilibrium molecular dynamics simulations of confined fluids in contact with the bulk. *J. Chem. Phys.*, **114**, 6869 (2001).
[18] E. Lauga, H.A. Stone. Effective slip in pressure-driven Stokes flow. *J. Fluid Mech.*, **489**, 55 (2003).
[19] G.C. Maitland, M. Rigby, E.B. Smith, W.A. Wakeham. *Intermolecular Forces*, p. 137, Oxford University Press, New York (1981).